Available online at www.sciencedirect.com

ScienceDirect

Trans. Nonferrous Met. Soc. China 21(2011) s262−s273

Transactions of Nonferrous Metals Society of China

www.tnmsc.cn

Aging and thermal expansion behavior of Si_3N_{4p}/2024Al composite fabricated by pressure infiltration method

CHEN Guo-qing[1], YANG Wen-shu[1, 2], MA Kang[1], Murid HUSSAIN [2], JIANG Long-tao[1], WU Gao-hui[1]

1. School of Materials Science and Engineering, Harbin Institute of Technology, Harbin 150001, China;
2. Department of Materials Science and Chemical Engineering, Politecnico di Torino, Turin 10129, Italy

Received 10 May 2011; accepted 25 July 2011

Abstract: The aging and thermal expansion behaviors of Si_3N_{4p}/2024Al composite fabricated by pressure infiltration method were investigated. The peak-aging time and peak hardness both decrease with the increase of aging temperature for both the 2024Al alloy and Si_3N_{4p}/2024Al composite. The calculated activation energies of *s*′ (precursors of the Al_2MgCu) phase indicate that the precipitation of *s*′ phase in Si_3N_{4p}/2024Al composite occurs easily than in 2024Al alloy. The presence of Si_3N_4 particles does not alter precipitation sequence, but accelerates the process of aging precipitation in Si_3N_{4p}/2024Al composite. The experimental coefficient of thermal expansion (CTE) of Si_3N_{4p}/2024Al composite bellow 100 °C is more close to the average value of the Kerner model (upper bound Schapery model) and lower bound Schapery model. Aging treated Si_3N_{4p}/2024Al composite presents the best dimensional stability due to low internal stress and strong pining effect on dislocations from fine dispersed precipitates (Al_2MgCu) and high density tangled dislocations. The good mechanical properties, compatible CTE with steel and high dimensional stability make Si_3N_{4p}/2024Al composite very competitive for application in the inertial guidance field.

Key words: Si_3N_4; Al matrix composite; aging; thermal expansion

1 Introduction

With the development of the aerospace technology, the dimensional stability of the materials used for the inertial instruments has become more and more important. Al alloys were used as the first generation inertial materials due to their excellent processing performance [1]. However, their large coefficient of thermal expansion (CTE) (21×10^{-6} °C^{-1}) and low elastic modulus (E≈70 GPa) cannot satisfy the increasing accuracy requirement. Beryllium was used for an inertial guidance device firstly in America as the second generation inertial materials [2−3] due to their high elastic modulus (E≈280 GPa) and similar CTE to steel (11.4×10^{-6} °C^{-1}). However, the application of beryllium was restricted because of its genotoxicity, carcinogenicity, high price and poor processing performance [4]. Recently, aluminum matrix composites reinforced with ceramic particulates were extensively investigated. These composites present high elastic modulus, high thermal conductivity, low density and low CTE [5]. These excellent properties make them very attractive for application in the inertial field. The micro-yield properties of Al_2O_{3p}/2024Al composite have been studied towards the application in inertial field [6].

Silicon nitride (Si_3N_4) has a good thermal and chemical stability, high mechanical strength and hardness, good wear, creep and corrosion resistance [7]. Theoretically, Si_3N_4 particles reinforced aluminum matrix composite (Si_3N_{4p}/Al) would present several advantages, including high specific strength, low thermal expansion, high thermal conductivity, high-intensity and good dimensional stability [8], which make them very promising for application in the inertial field.

Powder metallurgy technique [9−10], pressureless infiltration method [11−12], liquid metallurgy route [13] and pressure infiltration method [14−15] have been reported to fabricate Si_3N_{4p}/Al composite. Since wettability between Si_3N_4 particles and liquid aluminium is poor [16], pressure infiltration method seems to be a promising method to fabricate Si_3N_{4p}/Al composite with high density [17]. The researchers reported in the area of Si_3N_{4p}/Al composite have mainly focused on the

Foundation item: Project (20080430895) supported by China Postdoctoral Science Foundation; Project (2008RFQXG045) supported by Special Fund of Technological Innovation of Harbin, China; Project (HITQNJS.2009.021) supported by Development Program for Outstanding Young Teachers in Harbin Institute of Technology, China

Corresponding author: CHEN Guo-qin; Tel: +86-451-86402372-5058; E-mail: chenguoqin@hit.edu.cn

fabrication and characterization, and no literatures regarding the aging and thermal expansion behavior of Si_3N_{4p}/Al composite have been reported yet.

XIU et al [18] has reported the successful fabrication of 2024Al matrix composite reinforced with 45% (volume fraction) Si_3N_4 particles (Si_3N_{4p}/2024Al composite) with average particle size of 1.5 μm by pressure infiltration method, in which microstructure and tensile properties of Si_3N_{4p}/2024Al composite have been studied. This work is the continuation of the previous work [18]. In the present work, the aging behavior and microstructure of Si_3N_{4p}/2024Al composite were investigated by means of Brinell hardness measurement (HB), differential scanning calorimeter (DSC), scanning electron microscope (SEM) and transmission electron microscope (TEM). Thermal expansion behavior and dimensional stability of Si_3N_{4p}/2024Al composite were studied by means of CTE measurement and thermal cycling testing. The effect of the high volume fraction Si_3N_4 particles on the aging and thermal expansion behavior of the composite was deeply discussed.

2 Experimental

The Si_3N_4 particles (45%, volume fraction) with an average particle size of 1.5 μm were used to reinforce 2024Al alloy by pressure infiltration method, and the chemical composition (mass fraction, %) of the 2024Al alloy was 4.79% Cu, 1.49% Mg, 0.611% Mn, 0.245% Fe, 0.168% Si, 0.068% Zn, 0.049% Cr, 0.046% Ti, 0.013% Ni and Al balance. Figure 1 shows the flow chart for fabrication of experimental materials. The preheating temperatures for Si_3N_4 particle perform and squeeze casting dies were 500 and 740−750 °C, respectively. The matrix alloy was melted under protection of argon and melted salts, and poured into dies at 740−750 °C under argon. More details about microstructure and phases in Si_3N_{4p}/2024Al composite could be found in the previous work [18]. All specimens were solution treated at 495 °C for 1 h and then water quenched. The specimens were aged at 130, 160, 190 and 220 °C for periods up to 100 h, respectively. The hardness test results of 2024 matrix alloy have been reported by WANG et al [19] and the data were compared in the present work. After heat treatment, samples were stored at −20 °C to prevent possible natural aging.

The Brinell hardnesses of the specimens aged for different time at four temperatures were measured using HBV−30 A hardness testing machine. Five hardness measurements were made for each specimen to ensure the accuracy of results. Figure 2 shows the shape and dimensions of specimen used in hardness testing as well as the indented positions. DSC experiments were conducted on DSC−141 thermal analyzer (Setaram Company, France), and the mass of samples is less than 30 mg. All DSC tests were started at room temperature

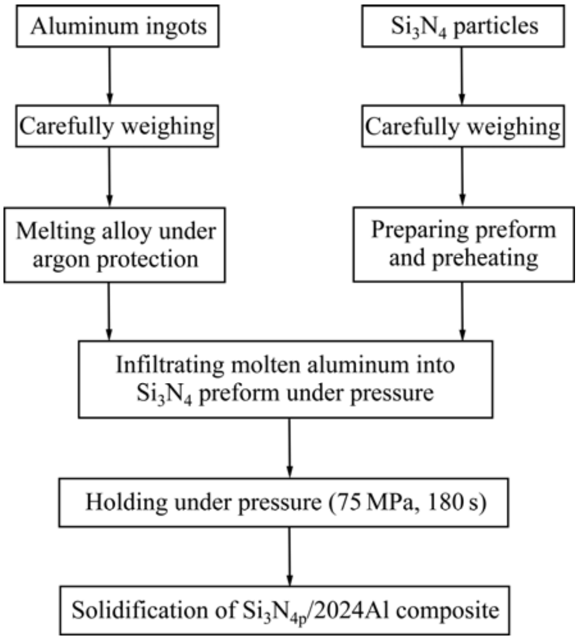

Fig. 1 Flow chart of pressure infiltration method used for fabricating Si_3N_{4p}/2024Al composite

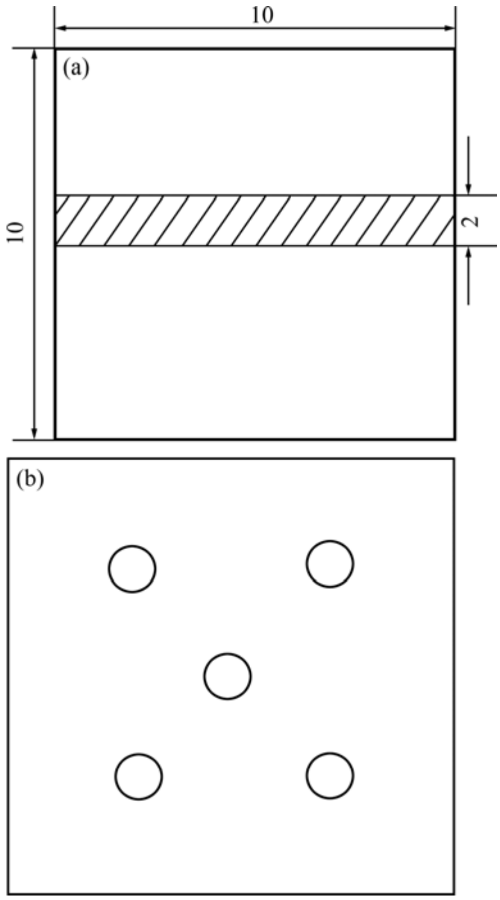

Fig. 2 Dimensions of hardness testing specimen (a) and indented positions (b) of hardness testing (mm)

and terminated at 400 °C at heating rates of 7.5, 10.0, 12.5, and 15.0 °C/min to study the activation energy of precipitates, respectively. Tensile samples (2 mm in thickness) were prepared from the composite and the dimensions are shown in Fig. 3. Room-temperature tensile test was conducted by Instron 5569 universal electrical tensile testing machine with the crosshead speed of 1 mm/min. The strain rate was 1.0 mm/min, according to Chinese National Standard GB/T 228—2002. Five specimens were tested and final values were obtained in terms of average value. Microstructure of composite was observed by a Philips CM−12 transmission electron microscope with an accelerated voltage of 100−120 kV.

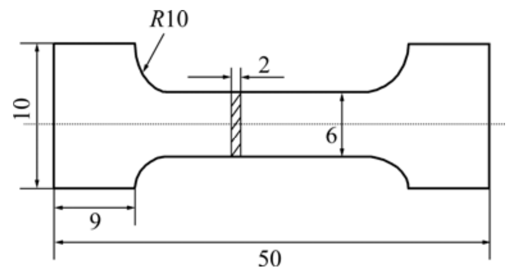

Fig. 3 Dimension of tensile sample (mm)

As-cast and peak-aging treated samples of Si_3N_{4p}/2024Al composite were tested for evaluation of the thermal expansion and dimensional stability. Peak-aging treated 2024Al alloy samples were also tested for comparison. The peak-aging temperature and time were determined by hardness and tensile strength test. The CTE measurement and thermal cycling test were both carried out on a Dilatometer 402C (Netzsch, Germany). The samples were the cylinders with a diameter of 4 mm and a length of 25 mm. During the CTE measurement, the temperature was heated from 20 to 500 °C at a heating rate of 5.0 °C/min. The helium atmosphere was maintained at a flow rate of 50 mL/min to ensure the equilibrium of temperature and prevent oxidation of samples. An average linear CTE was obtained according to

$$\alpha_{T,T_0} = \frac{\mathrm{d}l}{l_0 \cdot \mathrm{d}T} = \frac{l_T - l_0}{l_0 \cdot (T - T_0)} \quad (1)$$

where l_0 and l_T are referred to the length at temperatures T_0 and T, respectively. In this work, the CTE data were determined between 20 and 100 °C, with 50 °C intervals extending up to 500 °C. To diminish systematic errors, the dilatometer was calibrated by measuring an alumina sample under identical condition.

The samples were cycled between 20 and 150 °C for 15 complete cycles at heating and cooling rate of 8.0 °C/min. The helium atmosphere was maintained at a flow rate of 50 mL/min and liquid nitrogen was used as a coolant. The samples were maintained at 20 °C for 25 min before each cycle to ensure the equilibrium of temperature.

3 Results and discussion

3.1 Age hardening behavior

Figure 4 shows the hardness as a function of aging time for 2024Al alloy and Si_3N_{4p}/2024Al composite at 130, 160, 190 and 220 °C, respectively, while the data of 2024Al alloy were obtained from Ref. [19]. It has been observed that both in the as-quenched condition and in the subsequent aging process, the hardness of the composite is much higher than that of the matrix alloy. The reason is that the fine dispersed Si_3N_4 particles with high hardness can support the loading effectively due to their higher hardness. However, the hardness curves of Si_3N_{4p}/2024Al composite are not as smooth as Al matrix, which is also different to SiC_p/2024Al with same particle volume fraction of 45% [19], but the shapes of age hardening curves for the two materials are very similar. Hardness of the two materials increased firstly as a function of aging time before reaching peak hardness and then gradually decreased. It is worth noting that both in as-quenched condition and in the subsequent aging process, the hardness of Si_3N_{4p}/2024Al (above HB 380) is higher than SiC_p/2024Al (below HB 300) with the same particle volume fraction of 45% [19], even though the hardness of α-SiC particles (25 GPa) [20] is higher than that of β-Si_3N_4 particles (20 GPa) [21]. It makes Si_3N_{4p}/ 2024Al composite more attractive in field which requires a higher hardness.

The peak-aging time decreases with the increase of aging temperature for both the 2024Al alloy and Si_3N_{4p}/2024Al composite (Fig. 5(a)), and the time to achieve peak hardness is less in the Si_3N_{4p}/2024Al composite. This suggests that the high volume fraction of Si_3N_4 particles accelerates the aging kinetics of the composite matrix. Furthermore, the peak hardness also decreases with increase of aging temperature for both the 2024Al alloy and Si_3N_{4p}/2024Al composite (Fig. 5(b)) and the maximum hardness was obtained at aging temperature of 130 °C (HB 133 and HB 450 for 2024Al alloy and Si_3N_{4p}/2024Al composite, respectively). The trend is slightly different than the aging behavior of SiC_p/2024Al [18] and Al_2O_{3p}/2024Al [22], while the maximum hardnesses of both composites were obtained at aging temperature around 160 °C.

Figure 6 shows the tensile properties of Si_3N_{4p}/

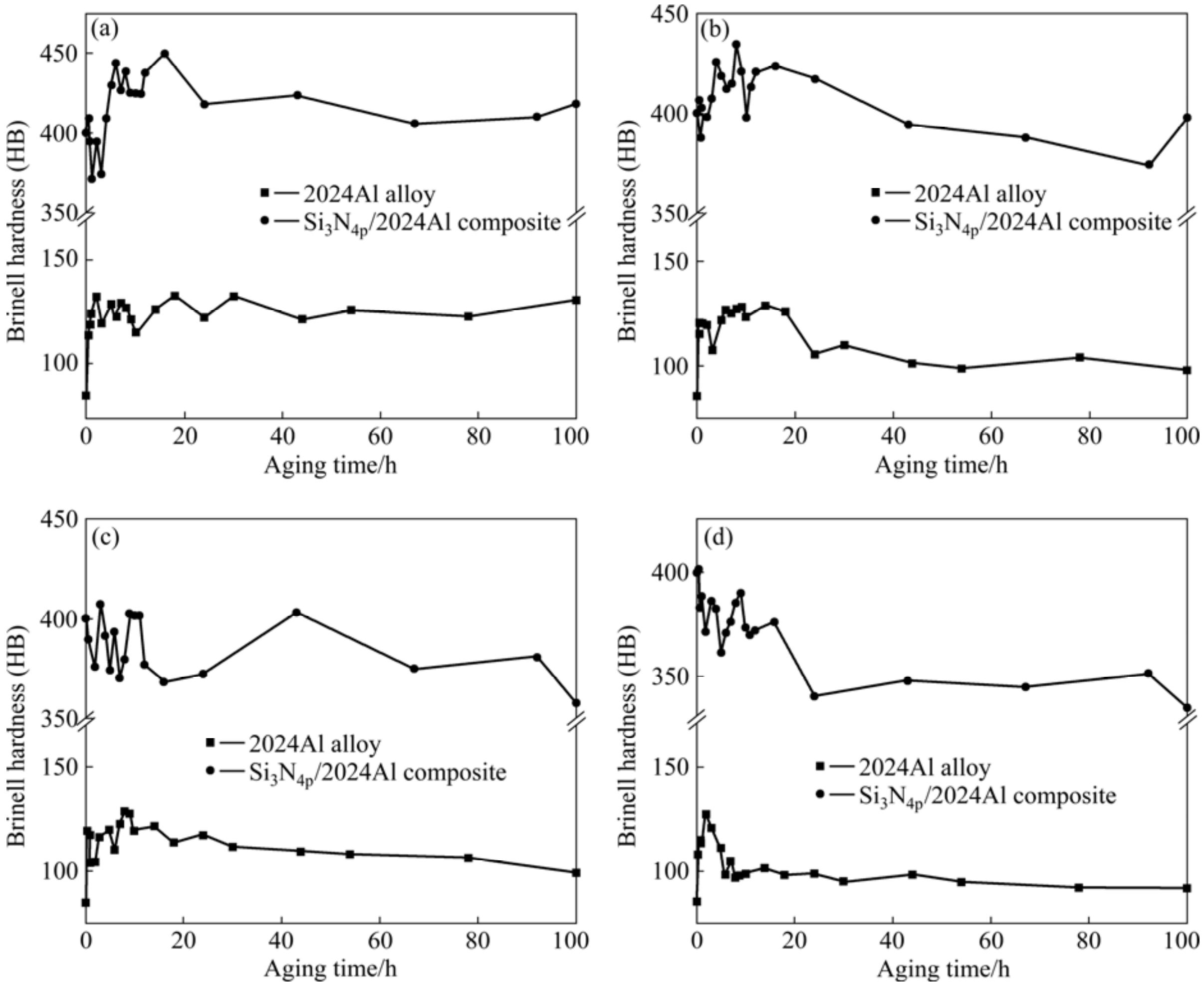

Fig. 4 Age hardening curves of Si_3N_{4p}/2024Al composite and 2024Al alloy aged at 130 °C (a), 160 °C (b), 190 °C (c) and 220 °C (d)

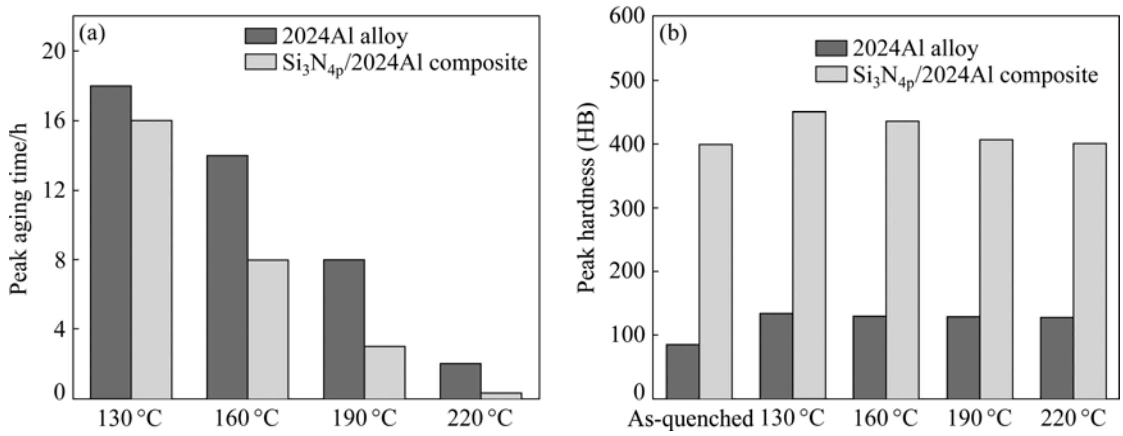

Fig. 5 Comparison of hardness results of aged Si_3N_{4p}/ 2024Al composite and 2024Al alloy: (a) Peak-aging time; (b) Peak hardness

2024Al composite after peak-aging treatment at 130, 160, 190 and 220 °C, respectively. The elastic modulus varies little with aging temperature, while tensile strength reaches the maximum (360 MPa) at 160 °C, which is different to hardness testing that the maximum of hardness is obtained at 130 °C, but is consistent with results in SiC_p/2024Al [19] and Al_2O_{3p}/2024Al [22]. However, higher temperature of aging treatment (190 and 220 °C) would decrease the tensile strength of Si_3N_{4p}/2024Al composite, which is consistent with the hardness testing results.

3.2 DSC analysis

The DSC thermograms of Si_3N_{4p}/2024Al composite

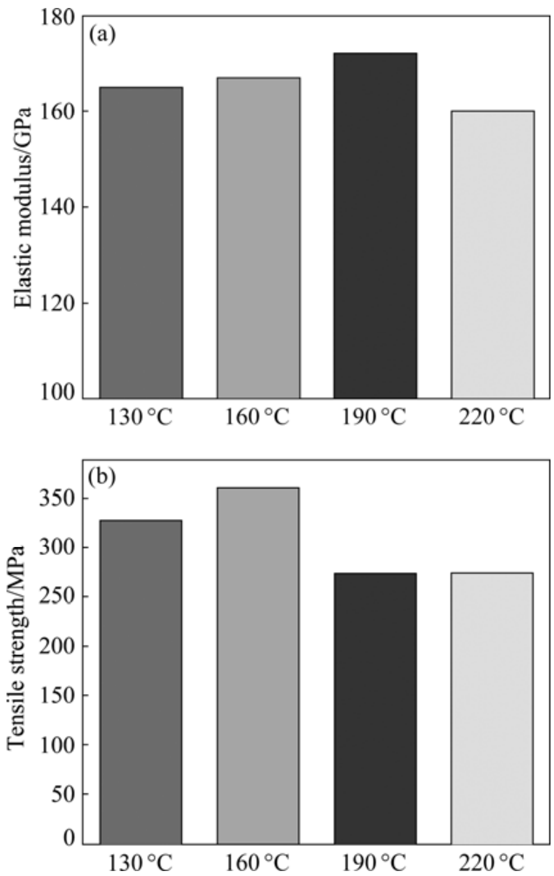

Fig. 6 Tensile properties of Si_3N_{4p}/2024Al composite after peak-aging treatment at 130, 160, 190 and 220 °C, respectively: (a) Elastic modulus; (b) Tensile strength

are obtained at different heating rates, as shown in Fig. 7. There is only one exothermic peak between the region of 200 and 250 °C. The mass ratio of Cu and Mg in the matrix alloy of the composite is in the range of 1.5−4.0. The balance phase is *s* phase (Al_2MgCu) and the precipitation process is: G.P zone→*s*′ phase→*s* phase [23]. Two clear exothermic peaks were observed in SiC_p/2024Al composite which corresponds to precipitation of *s*″ phase and *s*′ phase, respectively [19]. Only one exothermic peak between 200 and 250 °C was observed in Al_2O_{3p}/2024Al composite, which corresponded to the formation of *s*′ phase [22]. In the present work, *s*′ phase is the unique precipitate. This suggests that exothermic peak describes the formation of *s*′ phase.

To evaluate the effective activation energy, several models have been developed, such as Kissinger method [24], Augis and Bennett method [25] and Ozawa method [26]. Kissinger equation is the most commonly used model in analyzing the activation energy. This model describes the dependence of peak temperature on heating rate for a crystallization event by Eq. (2) [24]:

$$\ln\left(\frac{\beta}{T_p^2}\right) = -\frac{E_K}{RT_p} + \text{constant} \tag{2}$$

where T_p represents the exothermic peak temperature of precipitates; β represents the heating rate; E_K represents the Kissinger activation energy; R represents the gas constant equal to 8.314 J/(mol·K).

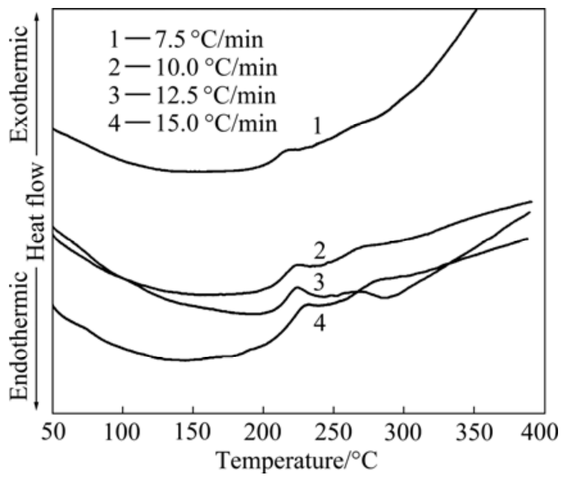

Fig. 7 DSC analysis of as-quenched Si_3N_{4p}/2024Al composites at different heating rates

The activation energy can also be determined by an approximation method developed by AUGIS and BENNETT [25] based on Eq. (3):

$$\ln\left(\frac{\beta}{T_p - T_{onset}}\right) = -\frac{E_{AB}}{RT_p} + \text{constant} \tag{3}$$

where T_{onset} and E_{AB} represent the onset temperature of precipitates and Augis-Bennett activation energy, respectively. The accuracy of T_{onset} evaluation is dependent on the accuracy of experimental recording of DSC curves. Therefore, AUGIS and BENNETT [25] have suggested a single value of T_0 lower than the minimum onset temperature to be used for all heating rates. Generally, consideration of T_{onset}=0 is used, and good agreements between values of E_{AB} and E_K have been obtained [27−28].

Another widely used method to determine the activation energy is, the Ozawa model [26], which is described as

$$\ln\beta = -\frac{E_o}{RT_p} + \text{constant} \tag{4}$$

where E_o represents the Ozawa activation energy.

The calculation data and results of Activation energies by Kissinger, Augis-Bennett and Ozawa models are listed in Table 1. The activation energies of *s*′ phase in Si_3N_{4p}/2024Al composite calculated by the above three models are lower than that of s' phase in 2024Al alloy. Therefore, the precipitation of s' phase in Si_3N_{4p}/2024Al composite occurs more easily than in 2024Al alloy, which accelerates precipitation process. It is consistent with hardness testing results (Fig. 5).

Table 1 Calculated activation energies of s' phase by different models

Material	Heating rate/ (°C·min^{-1})	Peak temperature/ °C	E_K/ (kJ·mol^{-1})	E_{AB}/ (kJ·mol^{-1})	E_o/ (kJ·mol^{-1})
2024Al	5	258.5	140.0	144.5	149.1
	10	268.6			
	15	274.2			
	20	281.8			
Si_3N_{4p}/ 2024Al	7.5	217.1	101.9	106.0	110.2
	10	222.2			
	12.5	223.9			
	15	230.2			

Note: The heating rates and peak temperature of 2024Al are from Ref. [19]

3.3 TEM Observation

Figure 8 shows the TEM microstructures of Si_3N_{4p}/2024Al composite aged at 160 °C for different periods. After aging for 2 h (under-aged), very fine precipitates were observed in the matrix alloy (Fig. 8(a)), and no apparent diffraction pattern was observed in electron diffraction patterns (EDP), as shown in Fig. 8(b). Prolonging aging time to 8 h (peak-aged), more fine precipitates were observed in the matrix alloy (Fig. 8(c)), and the hardness of Si_3N_{4p}/2024Al composite reached the maximum. Further aging to 100 h (over-aged), apparent needle-shaped precipitates were observed and coarsened remarkably (Fig. 8(e)). It can be seen from Fig. 8(f) that the weak diffraction spots in EDP are elongated to be lines and are identified to be Al_2MgCu.

The presence of high volume fraction of Si_3N_4 particles does not alter precipitation sequence, but accelerates the process of aging precipitation in Si_3N_{4p}/2024Al composite. The large coefficient of thermal expansion (CTE) difference between Si_3N_4 particles and Al matrix generates enormous thermal tensile stress and high density dislocations near the Si_3N_4-Al interface [18]. The high density dislocations would reduce the energy barrier of nucleation and the activation energy for phase formation, which accelerates the nucleation of precipitates. Moreover, high density dislocations can accelerate the growth of precipitates by enhancing the diffusion of solute atoms. The bulk diffusion coefficient of matrix alloy is not substantially affected by the addition of particles, but the pipe diffusion assisted by dislocations can be enhanced. However, the presence of high volume fraction of Si_3N_4 particles introduces a lot of interfaces into the composite, which would trap vacancies to reduce the whole concentration of vacancies in the matrix alloy. The decrease in concentration of vacancies has a strong suppress influence on the nucleation of G.P. zone, so no obvious peak associated with G.P. zone was observed in Si_3N_{4p}/2024Al composite.

3.4 Thermal expansion behavior

Figures 9(a) and (b) reveal the relative linear length change and CTE results with the variation of temperature for Si_3N_{4p}/2024Al composite and 2024Al alloy. The thermal expansion of 2024Al exceeds the measuring range of the equipment, which results in the platform above 450 °C as shown in Fig. 9(a). It has been observed that with the addition of high content of Si_3N_4 particles, the CTEs of Si_3N_{4p}/2024Al composite both in as-cast and aging treated conditions were reduced greatly to nearly half of the 2024Al matrix. It is well known that the thermal expansion of metal matrix composite is determined by the thermal expansion of metal matrix and the restriction of reinforcement through interfaces. High content of Si_3N_4 particles imposed large restriction on surrounding aluminum matrix, which leads to the low CTE of the Si_3N_{4p}/2024Al composite. Aging treatment could further decrease the CTE of the composite. Internal stress could be partially released during aging treatment, which leads to the decrease of CTE [29]. Moreover, after aging treatment, precipitates in Al matrix could also restrict the thermal expansion of Al matrix [19]. The CTE of Si_3N_{4p}/2024Al composite both in as-cast and aging treated conditions was about 10.4×10^{-6} °C^{-1} between 20 °C and 100 °C, which is compatible with steel. Hence, it makes Si_3N_{4p}/2024Al composite very attractive in the inertial field.

A number of models have also been developed for predicting the CTE of composite reinforced with particulates, and the most widely used models are Kerner [30], Schapery [31] and Turner models [32]. KERNER [30] assumed that the reinforcement was spherical and wetted by a uniform layer of matrix; and the CTE of the composite was stated to be identical to that of a volume element composed of a spherical reinforcement particle surrounded by a shell of matrix, while both phases having the volume fractions present in the composite. This model gives the composite CTE as

$$\begin{aligned}\alpha_c = \alpha_m V_m + \alpha_p V_p + V_p V_m (\alpha_p - \alpha_m)\cdot \\ (K_p - K_m)\cdot[V_m K_m + V_p K_p + (3K_p K_m / 4G_m)]^{-1}\end{aligned} \tag{5}$$

where α is the coefficient of thermal expansion; V is the volume fraction; K is the bulk modulus; G is the shear

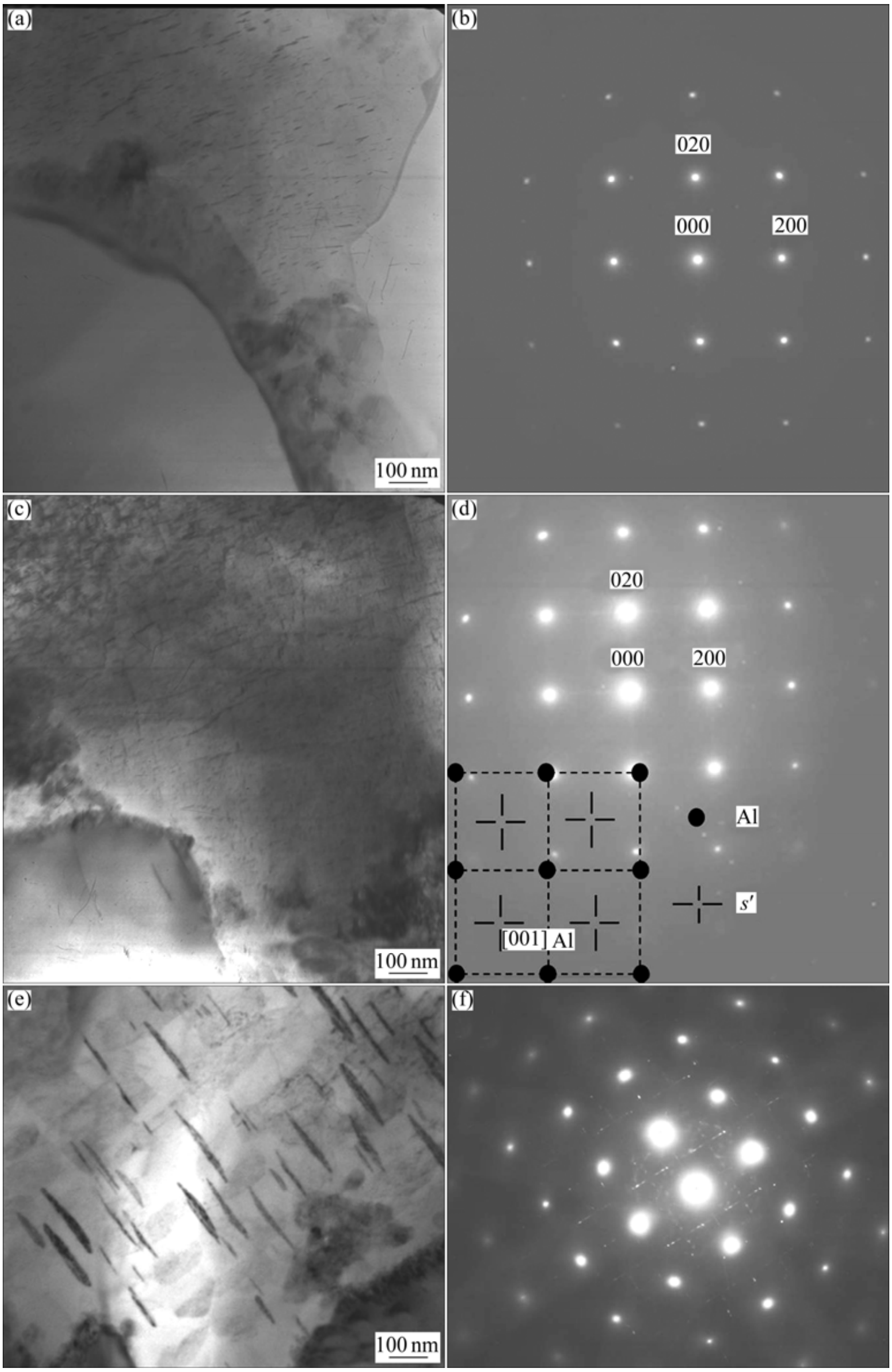

Fig. 8 Microstructures and EDP of Si_3N_{4p}/2024Al composites aged at 160 °C for different periods: (a), (b) 2 h; (c), (d) 8 h; (e), (f) 100 h

modulus; subscripts c, m and p refer to the composite, matrix and particles, respectively.

SCHAPERY [31] considered the stress interaction between components in composite and derived the effective CTE of isotropic composites by employing extremum principles of thermoelasticity as

$$\alpha_c = \alpha_p + (\alpha_m - \alpha_p) \times \frac{1/K_c - 1/K_p}{1/K_m - 1/K_p} \tag{6}$$

where α_c and K_c are the CTE and bulk modulus of the

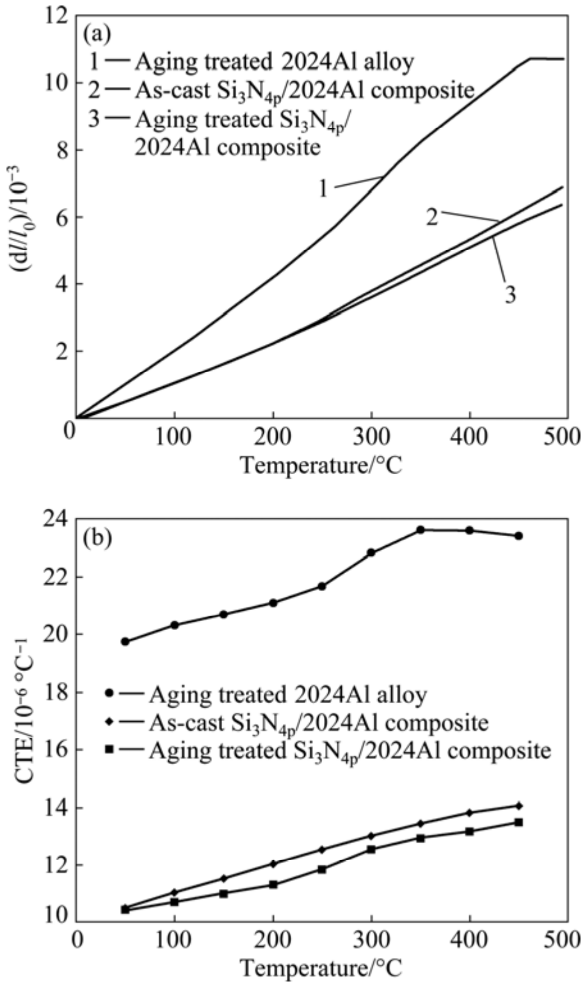

Fig. 9 Thermal expansion behavior of Si_3N_{4p}/2024Al composite and 2024Al alloy: (a) Relative linear length change with temperature; (b) CTE results

composite. Note that α_c depends on the volume fraction and phase geometry only through their effect on bulk modulus. This equation provides an exact relationship between composite CTE and bulk modulus. The upper bound of K_c is given by Eq. (7). It should be noted that the lower bound on K_c yields the upper bound on the CTE of composite (and vice versa).

$$K_c^{(+)} = K_p + V_m / [(K_m - K_p)^{-1} + V_p / (K_p + 4G_p / 3)] \quad (7)$$

The upper bound is obtained by interchanging the indices m and p everywhere. The lower bound of K_c yields the upper bound of the composite CTE (and vice versa). It should be noted that the upper bound of Schapery model coincides with the CTE value determined from Kerner's model.

TURNER [32] considered that the internal stress system in a mixture was such that the stresses were nowhere sufficient to disrupt the composite, the sum of the internal forces could be equated to zero and an expression for the CTE of the composite is obtained as

$$\alpha_c = \frac{\alpha_m V_m K_m + \alpha_p V_p K_p}{V_m K_m + V_p K_p} \quad (8)$$

Since the most of the particles used in the present work were β-Si_3N_4 [18], we just used the properties of β-Si_3N_4, and assumed that its properties do not change at low temperature [33]. The G and K data of β-Si_3N_4 particles were taken from Ref. [34] and the CTE data of β-Si_3N_4 particles were from Ref. [35]. The G and K data of 2024Al alloy were obtained from Ref. [33] and the CTE data of 2024Al alloy were from the present experiments. All the data used for calculation are listed in Table 2.

Table 2 Properties of β-Si_3N_4 particles and 2024Al alloy

t/°C	β-Si_3N_4 particle			2024Al alloy		
	G/GPa	K/GPa	CTE/ 10^{-6} °C^{-1}	G/GPa	K/GPa	CTE/ 10^{-6} °C^{-1}
50	122	234	3.3	27.2	68.28	19.8
100	122	234	3.3	26.6	68.55	20.7
200	122	234	3.3	24.7	66.21	21.1
300	122	234	3.3	24.1	59.79	22.9
400	122	234	3.3	18.1	60.96	23.6

The CTE comparison between theoretical calculations and experimental results of Si_3N_{4p}/2024Al composite is shown in Fig. 10. The experimental CTE bellow 100 °C is more close to the average value of the Kerner model (upper bound by Schapery model) and lower bound by Schapery model. However, above 100 °C, the experimental CTE agrees well with the values predicted by the Kerner model. This indicates that the stress interaction between components in composite plays an important role in thermal expansion behavior of Si_3N_{4p}/2024Al composite at low temperature. ZHANG et al [36] reported that at room temperature, Kerner model (8.1×10^{-6} °C^{-1}) was in good agreement with the experimental CTE (7.3×10^{-6} °C^{-1}) for 73% (volume fraction) SiC_p/2024Al composite fabricated by pressure infiltration method. However, the CTE calculated by lower bound of Schapery model is 7.1×10^{-6} °C^{-1}. It seems that the experimental results of ZHANG et al [37] are more close to the average value (7.6×10^{-6} °C^{-1}) of Kerner model (upper bound of Schapery model) and lower bound of Schapery model, which is the same as the present work. ELOMARI et al [33] examined the 55% (volume fraction) SiC_p/Al composite and found that the experimental CTE agreed well with the values predicted by upper bound of Schapery model at low temperatures (50−150 °C), and did not agree with any of the theories at high temperature, which is slightly different than the present work.

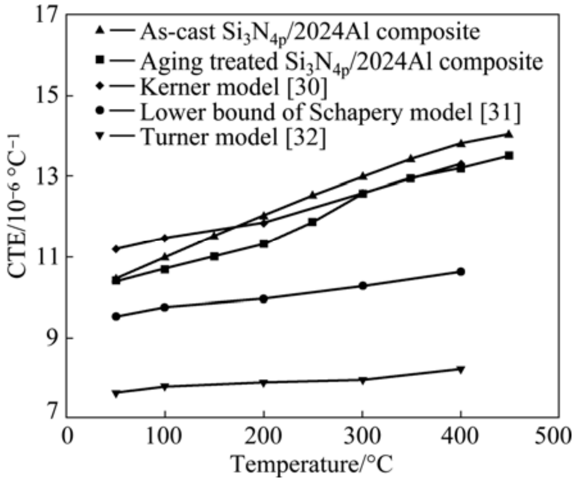

Fig. 10 CTE comparison between theoretical calculation and experimental results of Si_3N_{4p}/2024Al composite

3.5 Thermal cycling

The relative length change (ε) during thermal cycling of aging treated 2024Al, as-cast and aging treated Si_3N_{4p}/2024Al composites is shown in Figs. 11(a), (b) and (c), respectively. The relative length change of 2024Al alloy is almost two times larger than that of Si_3N_{4p}/2024Al composite. It is due to the fact that the CTE of Si_3N_{4p}/2024Al composite is almost half that of 2024Al alloy.

The residual length change (Δ_i) at 20 °C is calculated from strain−time curves by Eq. (9):

$$\Delta_i = \varepsilon_{\rm i} - \varepsilon_0 \tag{9}$$

where ε_0 is the original length change at 20 °C (the first platform before thermal cycling), and ε_i refers to the sample length at the same temperature after i cycles (the following platform). The magnitude of Δ_i represents the accumulative residual length change after i cycles.

Figure 12 shows the relationship between Δ_i and cycling number of aging treated 2024Al, as-cast and aging treated Si_3N_{4p}/2024Al composites. Since the thermal cycling behaviors of three materials are different, they will be discussed separately.

Aging treated 2024Al presents a progressive increase in the residual length change with cycling. Although a large amount of internal stress has been released during aging treatment, there is still a small stress in Al alloy. Since the strength of Al matrix is low and decreases sharply with increasing temperature, movement of dislocations could occur during thermal cycling, which leads to permanent deformation of Al alloy [37]. Actually, the increase of residual length was even observed in pure Al [38], and TJONG et al [38] attributed it to the internal stress arising from temperature difference from interior to surface of the sample. Moreover, the volume expansion caused by precipitation also contributes to the increase of sample length [39].

As-cast Si_3N_{4p}/2024Al composite shows a progressive decrease in residual length change with cycling. The first cycling makes a significant contribution, and the contributions of subsequent cycles decrease with cycle number. In the Si_3N_{4p}/2024Al

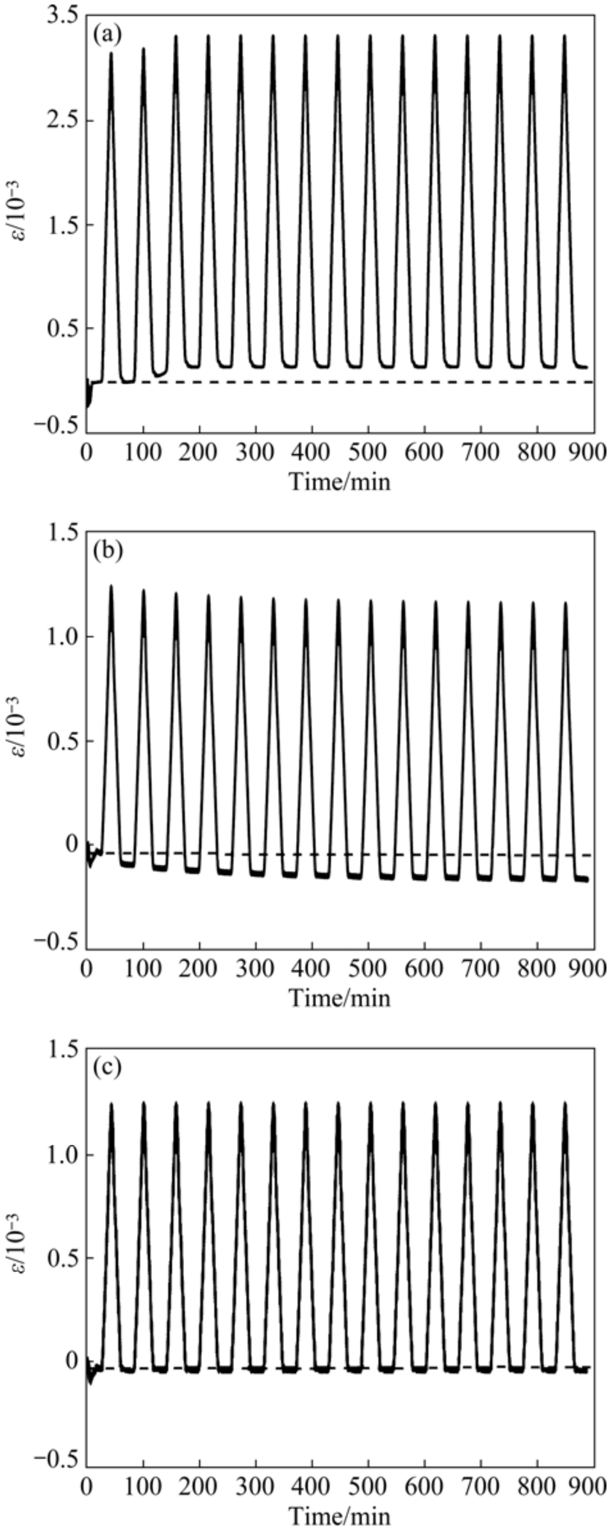

Fig. 11 Relative length change during thermal cycling of aging treated 2024Al (a), as-cast Si_3N_{4p}/2024Al composite (b) and aging treated Si_3N_{4p}/2024Al composite (c)

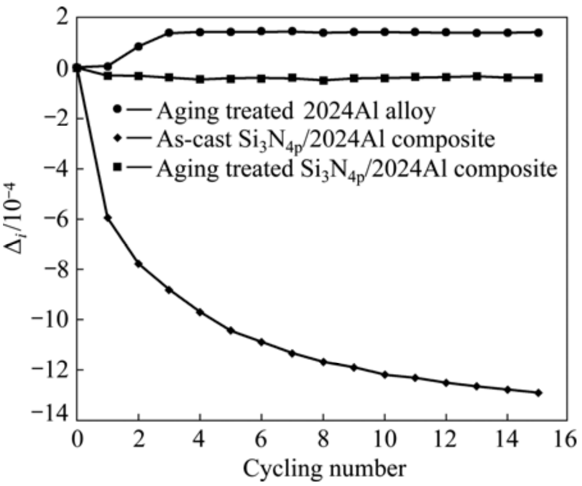

Fig. 12 Relationship between residual relative length change (Δ_i) and cycling number of aging treated 2024Al alloy, as-cast and aging treated Si_3N_{4p}/2024Al composite

composite, due to the CTE mismatch between the reinforcement (3.3×10^{-6} °C^{-1}) and Al matrix (22×10^{-6} °C^{-1}), a large internal thermal stress could be introduced into during fabrication or subsequent processing. These thermal residual stresses are tensile in the Al matrix and compressive in Si_3N_4 particles. Reheating the composite, initially, the residual stress is expected to relax elastically with increase of temperature. The yield strength of matrix alloy drops sharply with temperature. It may be due to the fact that the thermal stress in the composite matrix exceeds the yield strength of the matrix alloy at a certain temperature, causing the appearance of a plastic deformation under compressive stress. The yielding of composite matrix causes the appearance of a plastic strain component (negative) which will be superimposed to the thermal strain (positive during heating cycle), leading to the large length decrease of Si_3N_{4p}/2024Al composite after the first thermal cycling [40]. However, at a low cycling temperature (150 °C), only part of internal stress could be released. During subsequent cycling, the other internal stress would be released gradually, which results in the progressive decrease in residual length. Apparently, the entire residual stress is not released even after 15 cycles. Furthermore, the contribution of subsequent cycles decreases with cycle number due to the following two factors: 1) a decreased initial stress as a result of the partial relief of stresses during the previous cycling; 2) the working hardening effect induced by the plastic deformation [35].

Aging treated Si_3N_{4p}/2024Al composite presents the best dimensional stability, which is an order of magnitude lower than that of 2024Al matrix. It makes Si_3N_{4p}/2024Al composite very competitive for application in the inertial guidance field. After aging treatment, the internal thermal stress is very small in Si_3N_{4p}/2024Al composite. Furthermore, the fine dispersed Al_2MgCu precipitates (Fig. 8(c)) and high density tangled dislocations [18] in Al matrix, are beneficial in pinning the dislocations and increasing the yield strength of Al matrix. This leads to a very small residual length change after thermal cycling. The compatible CTE with steel and high dimensional stability makes Si_3N_{4p}/2024Al composite very competitive for application in inertial guidance field.

4 Conclusions

1) The aging and thermal expansion behaviors of Si_3N_{4p}/2024 composite fabricated by pressure infiltration method were investigated. The maximum hardness of Si_3N_{4p}/2024Al composite is HB 450. The peak-aging time and peak hardness both decrease with increase of aging temperature for both the 2024Al alloy and Si_3N_{4p}/2024Al composite. Tensile strength reaches the maximum of 360 MPa at aging temperature of 160 °C. The activation energies of s' phase were calculated by Kissinger, Augis-Bennett and Ozawa models, which indicate the precipitation of s' phase in Si_3N_{4p}/2024Al composite occurs more easily than in 2024Al alloy. TEM observation shows that the presence of high volume fraction of Si_3N_4 particles does not alter precipitation sequence, but accelerates the process of aging precipitation in Si_3N_{4p}/2024Al composite.

2) The CTE of Si_3N_{4p}/2024Al composite is 10.4×10^{-6} °C^{-1} between 20 °C and 100 °C. Internal stress could be partially released after aging treatment, which further decreases the CTE of Si_3N_{4p}/2024Al composite. The experimental CTE of Si_3N_{4p}/2024Al composite bellow 100 °C is more close to the average value of the Kerner model (upper bound Schapery model) and lower bound of Schapery model. Aging treated 2024Al presents a progressive increase in residual length change due to permanent deformation of Al alloy. As-cast Si_3N_{4p}/2024Al composite shows a progressive decrease in residual length change with cycling due to release of internal stress. Aging treated Si_3N_{4p}/2024Al composite presents the best dimensional stability due to a low internal stress and strong pining effect on dislocations from fine dispersed precipitates (Al_2MgCu) and high density tangled dislocations. The good mechanical properties, compatible CTE with steel and high dimensional stability makes Si_3N_{4p}/2024Al composite

very competitive for application in the inertial guidance field.

References

[1] BEGG A R. Applications for metal matrix composites [J]. Metal Powder Report, 1991, 46(10): 42−45.

[2] DUNCAN R C, GUNNERSEN A S. Inertial guidance, navigation, and control systems [J]. Journal of Spacecraft and Rockets, 1964, 1(6): 577−587.

[3] SOFFA L L. Nondestructive testing of hot pressed beryllium for inertial instrument applications [J]. Nondestructive Testing, 1962, 20: 242−244.

[4] GORDON T, BOWSER D. Beryllium: Genotoxicity and carcinogenicity [J]. Mutation Research, 2003, 533: 99−105.

[5] ZHANG Q, WU G H, JIANG L T. Tensile deformation behavior of a sub-micrometer Al_2O_3/6061Al composite [J]. Materials Science and Engineering A, 2008, 483−484: 281−284.

[6] WANG X F, WU G H, SUN D L, QIN C J, TIAN Y L. Micro-yield property of sub-micron Al_2O_3 particle reinforced 2024 aluminum matrix composite [J]. Materials Letters, 2004, 58: 333−336.

[7] YE F, ZHANG J Y, LIU L M, ZHAN H J. Effect of solid content on pore structure and mechanical properties of porous silicon nitride ceramics produced by freeze casting [J]. Materials Science and Engineering A, 2011, 528: 1421−1424.

[8] IWASAKI H, MABUCHI M, HIGASHI K, LANGDON T G. The development of cavitation in superplastic aluminum composite reinforced with Si_3N_4 [J]. Materials Science and Engineering A, 1996, 208: 116−121.

[9] ARIK H. Effect of mechanical alloying process on mechanical properties of α-Si_3N_4 reinforced aluminum-based composite materials [J]. Materials and Design, 2008, 29: 1856−1861.

[10] JEONG H G, HIRAGA K, MABUCHI M, HIGASHI K. Effect of addition of magnesium on interface structure and high-stain-rate superplasticity in Si_3N_4 reinforced Al-alloy composite [J]. Acta Metallurgica, 1998, 46: 6009−6020.

[11] FARID A, GUO Shi-ju. Development of Si_3N_4/Al composite by pressureless melt infiltration [J]. Transaction of Nonferrous Metals Society of China, 2006, 16: 629−632.

[12] WANG S R, WANG Y Z, WANG Y, GENG H R, CHI Q. Microstructure and infiltration kinetics of Si3N4/Al-Mg composite fabricated by pressureless infiltration [J]. Journal of Materials Science, 2007, 42: 7812−7818.

[13] RAMESH C S, KESHAVAMURTHY R, CHANNABASAPPA B H, AHMED A. Microstructure and mechanical properties of Ni-P coated Si_3N_4 reinforced Al6061 composite [J]. Materials Science and Engineering A, 2009, 502: 99−106.

[14] YANG Wen-shu, XIU Zi-yang, CHEN Guo-qin, WU Gao-hui. Microstructure and thermal conductivity of submicron Si_3N_4 reinforced 2024Al composite [J]. Transaction of Nonferrous Metals Society of China, 2009, 19(s): s378−s381.

[15] PENG L M, HAN K S, CAO J W, NADA K. Fabrication and mechanical properties of high-volume-fraction Si_3N_4-Al-based composite by squeeze infiltration casting [J]. Journal of Materials Science Letters, 2003, 22: 279−282.

[16] de la PEŇA J L, PECH-CANNUL M I. Reactive wetting and spreading of Al-Si-Mg alloys on Si_3N_4/Si substrates [J]. Materials Science and Engineering A, 2008, 491(1−2): 461−469.

[17] XIU Zi-yang, CHEN Guo-qin, LIU Yan-mei, YANG Wen-shu, WU Gao-hui. Effects of extrusion deformation on mechanical properties of sub-micron Si_3N_{4p}/2024 composite [J]. Transaction of Nonferrous Metals Society of China, 2009, 19(s): s373−s377.

[18] XIU Z Y, YANG W S, CHEN G Q, JJANG L T, MA K, WU G H. Microstructure and tensile properties of Si_3N_{4p}/2024Al composite fabricated by pressure infiltration method [J]. Materials and Design, 2012, 33: 350−355.

[19] WANG X F, WU G H, SUN D L, JIANG L T, HAN Y Y. Aging behavior of high volume fraction SiC particles reinforced 2024Al composite [J]. Journal of Materials Science and Technology, 2004, 20(2): 167−172.

[20] YONENEGA I. Thermo-mechanical stability of wide-bandgap semiconductors: High temperature hardness of SiC, AlN, GaN, ZnO and ZnSe [J]. Physica B, 2001, 308−310: 1150−1152.

[21] OTAGA S, HIROSAKI N, KOCER C, SHIBUTANI Y. A comparative ab initio study of the 'ideal' strength of single crystal α- and β-Si_3N_4 [J]. Acta Metallurgica, 2004, 52: 233−238.

[22] JIANG L T, ZHAO M, WU G H, ZHANG Q. Aging behavior of sub-micron Al2O3P/2024Al composites [J]. Materials Science and Engineering A, 2005, 392: 366−372.

[23] PAREL T S, WANG S C, STARINK M J. Hardening of an Al-Cu-Mg alloy containing types I and II *S* phase precipitates [J]. Materials and Design, 2010, 31: s2−s5.

[24] KISSINGER H E. Variation of peak temperature with heating rate in differential thermal analysis [J]. Journal of Research of the National Bureau of Standards, 1956, 57: 217–221.

[25] AUGIS J A, BENNETT J E. Calculation of the Avrami parameters for heterogeneous solid state reactions using a modification of the Kissinger method [J]. Journal of Thermal Analysis, 1978, 3: 283–292.

[26] OZAWA T. A new method of analyzing thermogravimetric data [J]. Bulletin of the Chemical Society of Japan, 1965, 38: 1881–1886.

[27] JOSEPH K, VENKATA KRISHNAN R, GOVINDAN KUTTY K V, VASUDEVARAO P R. Crystallisation kinetics of a cesium iron phosphate glass [J]. Thermochimica Acta, 2009, 494: 110–114.

[28] BISWAS K, SONTAKKE A D, MAJUMDER M, ANNAPURNA K. Nonisothermal crystallization kinetics and microstructure evolution of calcium lanthanum metaborate glass [J]. Journal of Thermal Analysis and Calorimetry, 2010, 101: 143–151.

[29] CHEN Guo-qin, XIU Zi-yang, YANG Wen-shu, JIANG Long-tao, WU Gao-hui. Effect of thermal-cooling cycle treatment on thermal expansion behavior of particulate reinforced aluminum matrix composites [J]. Transaction of Nonferrous Metals Society of China, 2010, 20: 2143–2147.

[30] KERNER E H. The elastic and thermo-elastic properties of composite media [J]. Proceedings of the Physical Society, 1956, 69: 808–815.

[31] SCHAPERY R A. Thermal expansion coefficients of composite materials based on energy principles [J]. The Journal of Composite Materials, 1968, 2: 380–404.

[32] TURNER P S. Thermal expansion stresses in reinforced plastics [J]. Journal of Research of the National Bureau of Standards, 1946, 37: 239–250.

[33] ELOMARI S, SKIBO M D, SUNDARRAJAN A, RICHARDS H. Thermal expansion behavior of particulate metal-matrix composites [J]. Composites Science and Technology, 1998, 58: 369–376.

[34] YEHESKEL O, GEFEN Y. The effect of the α phase on the elastic properties of Si_3N_4 [J]. Materials Science and Engineering A, 1985, 71: 95–99.

[35] YE F, CHEN S, IWASA M. Synthesis and mechanical properties of 40 wt%BAS/Si_3N_4 ceramic composites [J]. Journal of Materials Science Letters, 2003, 22: 895–897.

[36] ZHANG Q, WU G H, JIANG L T, CHEN G Q. Thermal expansion and dimensional stability of Al-Si matrix composite reinforced with high content SiC [J]. Materials Chemistry and Physics, 2003, 82: 780–785.

[37] KUMAR S, MONDAL A K, DIERINGA H, KAINER K U.

Analysing hysteresis and residual strains in thermal cycling curves of short fibre reinforced Mg-MMCs [J]. Composites Science and Technology, 2004, 64: 1179–1189.
[38] TJONG S C, TAM K F, WU S Q. Thermal cycling characteristics of in-situ Al-based composites prepared by reactive hot pressing [J]. Composites Science and Technology, 2003, 63: 89−97.
[39] JIANG Long-tao, WU Gao-hui, YANG Wen-shu, ZHAO Yong-gang, LIU Shan-shan. Effect of heat treatment on microstructure and dimensional stability of ZL114A aluminum alloy [J]. Transaction of Nonferrous Metals Society of China, 2010, 20(11): 2124–2128.
[40] HUANG Y D, HORT N, DIERINGA H, KAINER K U. Analysis of instantaneous thermal expansion coefficient curve during thermal cycling in short fiber reinforced $AlSi_{12}CuMgNi$ composites [J]. Composites Science and Technology, 2005, 65: 137–147.

压力浸渗法制备 Si_3N_{4p}/2024Al 复合材料的时效和热膨胀行为

陈国钦[1]，杨文澍[1,2]，马 康[1]，Murid HUSSAIN[2]，姜龙涛[1]，武高辉[1]

1．哈尔滨工业大学 材料科学与工程学院，哈尔滨 150001；
2．Department of Materials Science and Chemical Engineering, Politecnico di Torino, Turin 10129, Italy

摘 要：采用压力浸渗法制备 Si_3N_{4p}/2024Al 复合材料，并研究其时效和热膨胀行为。2024 铝合金和 Si_3N_{4p}/2024Al 复合材料的峰时效时间及硬度均随着时效温度的升高而降低。激活能计算结果表明，在 Si_3N_{4p}/2024Al 复合材料中 s'相析出比在 2024 铝合金中容易。Si_3N_4 的加入，未改变析出相的析出顺序，但是加速了析出。在低于 100 °C 时，Si_3N_{4p}/2024Al 复合材料的热膨胀系数接近 Kerner 模型(即 Schapery 模型的上限)和 Schapery 模型的下限的平均值。由于低的内应力、弥散分布的 Al_2MgCu 析出相对位错的强钉扎作用以及高密度缠绕的位错，时效处理后的 Si_3N_{4p}/2024Al 复合材料具有最好的尺寸稳定性。由于具有良好的力学性能和钢匹配的热膨胀数系以及优异的尺寸稳定性，Si_3N_{4p}/2024Al 复合材料在惯性导航领域具有广阔的应用前景。

关键词：Si_3N_4；铝基复合材料；时效；热膨胀

(Edited by LI Xiang-qun)